JAM CM Journal of Applied Mathematics and Computational Mechanics 2022, 21(2), 15-26
www.amcm.pcz.pl p-ISSN 2299-9965
DOI: 10.17512/jamcm.2022.2.02 e-ISSN 2353-0588

DEVELOPMENT OF MATHEMATICAL AND NUMERICAL MODELS FOR THE ANALYSIS OF OVERLAP LASER BEAM WELDING OF DISSIMILAR MATERIALS

Tomasz Domański[1], Wiesława Piekarska[2], Zbigniew Saternus[1], Marcin Kubiak[1]

[1] Department of Mechanical Engineering and Computer Science
Czestochowa University of Technology, Czestochowa, Poland
[2] Faculty of Architecture, Civil Engineering and Applied Arts, University of Technology
Katowice, Poland
tomasz.domanski@pcz.pl, wieslawa.piekarska@pcz.pl, zbigniew.saternus@pcz.pl
marcin.kubiak@pcz.pl

Received: 12 January 2022; Accepted: 15 April 2022

Abstract. The welding process of dissimilar materials causes a lot of technological issues related to different properties of materials of joined elements. Thermal conductivity is one of most important factors influencing the deformation of the weld. The change of thermal conductivity in the function of the temperature can produce various strains that cannot be predicted during construction design. Different structures of materials appear during joining of dissimilar materials as well as different characteristic zones of the joint and its mechanical properties. The most important is the proper identification of joint zones and the size of deformation at the production stage of welded construction. This work presents the numerical analysis of physical phenomena in overlap welding of two sheets made of S355 carbon steel and 304 austenitic steel using a laser beam. A three-dimensional discrete model is developed taking into account thermophysical properties changing with temperature. Temperature distribution and the shape of the welding pool is predicted on the basis of performed computer simulations. The influence of thermal load on the formation of stress and strain fields is determined.

MSC 2010: *65E05, 80A05*
Keywords: *mathematical and numerical modelling, dissimilar materials, laser welding, thermomechanical phenomena*

1. Introduction

The overlap welding method using a laser beam is widely used in the industry [1-3]. In this process, the laser beam penetrates the top surface of the upper flat bar and blends into the lower element. This method of joining materials is also used in the case of welding of dissimilar materials [4-7]. In recent years, the method of

joining dissimilar materials has become increasingly used in many fields of the industry [8-10]. The major demand for this type of joints occurs in the aerospace and energy industry. It is caused by the desire to reduce production costs while maintaining the same strength properties. The process of joining dissimilar materials is difficult to perform due to three main factors affecting the weldability of these materials [11, 12]. These factors are the melting point, chemical composition, and thermal conductivity [13, 14]. The proper process parameters are difficult to achieve. Experimental studies are often performed, but they are time consuming and costly. Therefore, at an early design stage, numerical modelling is used [9, 15-17]. However, such estimation studies at the final stage of the numerical model development need to be verified on the basis of experimental studies [7-9]. During the analysis, the best process parameters can be estimated and the influence of these parameters on the fusion zone, stress state and joint deformation can be determined [17]. Currently, scientific publications in the field of laser welding of dissimilar materials cover mostly experimental research [1, 6-8]. There are only few papers with mathematical and numerical models describing phenomena occurring during welding of dissimilar materials. This work concerns the development of numerical models and computer simulations performed on the basis of the results of the real welding tests.

The paper presents numerical prediction of deformation in a laser welded lap joint. In the welding process, two different materials are assumed: 304 austenitic steel and S355 high-strength steel. Numerical calculations are performed using finite element method, implemented into Abaqus FEA solvers. Changing with temperature thermophysical properties are defined for joined materials. Additional numerical subroutines are implemented in FORTRAN programming language in order to adapt the Abaqus FEA for numerical simulations of the welding process. Appropriate thermal and mechanical contact conditions are defined in the area of joint and the area of overlapping of connected steel sheets. The influence of the assumed thermal load on the stress state and deformation is analysed. On the basis of performed simulations, the temperature distributions in the lap joint determined, as are the fusion zone, stress state and deformations.

2. Mathematical model

Numerical analysis of thermal phenomena in Abaqus software is based on the basic energy balance equation (Green and Naghdi equation)

$$\int_V \rho \dot{U}\, dV = \int_S q\, dS + \int_V r\, dV \tag{1}$$

where V is a volume of solid material with surface area S; ρ is the density of the material; $\dot{U}$ is the material time rate of the internal energy; q is the heat flux per unit area of the body, flowing into the body; and r is the heat supplied internally

into the body per unit volume. Heat conduction is assumed to be governed by the Fourier law:

$$f = -k\frac{\partial T}{\partial x} \tag{2}$$

where k is the conductivity matrix, $k = k(T)$; f is the heat flux; and x is position.

Equation (1) with Fourier law (2) is solved using the finite element method. The "week form" of weighted residuum method is described as follows [11]:

$$\int_V \rho\frac{\partial U}{\partial t}\delta T dV + \int_V \frac{\partial \delta T}{\partial x_\alpha}\cdot\left(\lambda\frac{\partial T}{\partial x_\alpha}\right)dV = \int_V \delta T\, q_V dV + \int_S \delta T\, q_S dS \tag{3}$$

where λ is a thermal conductivity [W/m K], $U = U(T)$ is an internal energy [J/kg], q_v is a laser beam heat source [W/m^3], $T = T(x_\alpha,t)$ is a temperature [K], q_s is a boundary heat flux [W/m^2], δT is a variational function, ρ is a density [kg/m^3], $T = T(x_\alpha,t)$ is temperature [K].

Numerical simulation is performed in Lagrange coordinates. The location of the heat source center $x_0 = v\cdot t$ is determined for each time t [s] depending on the adopted speed v [m/s]. The heat transfer equation (3) is supplemented by initial conditions and boundary conditions of Dirichlet, Neumann and Newton types. The loss of heat to the environment is modelled by convection, radiation and evaporation [15, 18, 19], according to the following formula:

$$q_S = -\lambda\frac{\partial T}{\partial n} = -q(r,0) + \alpha_k(T\big|_\Gamma - T_0) + \varepsilon\sigma(T\big|_\Gamma{}^4 - T_0^4) \tag{4}$$

where α_k is convective coefficient, ε is radiation coefficient ($\varepsilon = 0.5$), σ is Stefan-Boltzmann constant and $q(r,0)$ is the heat flux towards the top surface of welded workpiece ($z = 0$) in the source activity zone of radius r, T_0 is an ambient temperature.

Internal energy U in equation (3) takes into account the latent heat of fusion (H_L) in the mushy zone between T_S (solidus temperature) and T_L (liquidus temperature). Therefore, changes in specific heat $c(T) = dU/dT$ [J/(kg K)] are defined as:

$$c(T) = \begin{cases} c_S & \text{for} \quad T < T_S \\ \dfrac{c_S + c_L}{2} + \dfrac{H_L}{(T_L - T_S)} & \text{for} \quad T_S \le T \le T_L \\ c_L & \text{for} \quad T > T_L \end{cases} \tag{5}$$

where c_S, c_L are specific heat in solid and liquid phase.

The classical, literature model of the volumetric, moveable heat source (q_v) is used for the mathematical description of the laser beam power intensity. Heat source power distribution in radial direction is defined by Gaussian model [17, 20].

The model assumes a linear decrease in energy with the penetration depth of the welded material [15, 17]. The movable heating source in the computing program is modelled using additional subroutines DFLUX, loaded into the computing solver.

Calculations of mechanical phenomena are carried out in the elastic-plastic range and are based on equilibrium equations (6) [18, 19, 21]. Governing equations are supplemented by constitutive relations describing the relationship between stresses and strains [21].

$$\nabla \circ \dot{\boldsymbol{\sigma}}\left(x_\alpha, t\right) = 0, \qquad \dot{\boldsymbol{\sigma}} = \dot{\boldsymbol{\sigma}}^T \tag{6}$$

$$\dot{\boldsymbol{\sigma}} = \mathbf{D} \circ \dot{\boldsymbol{\varepsilon}}^e + \dot{\mathbf{D}} \circ \boldsymbol{\varepsilon}^e, \boldsymbol{\varepsilon}^{total} = \boldsymbol{\varepsilon}^e + \boldsymbol{\varepsilon}^p + \boldsymbol{\varepsilon}^{Th} \tag{7}$$

where $\boldsymbol{\sigma} = \boldsymbol{\sigma}(\sigma_{ij})$ is a Cauchy stress tensor, x_α is the location of a considered point, $\mathbf{D} = \mathbf{D}(T)$ is a stiffness matrix, total strain rate ε^{total} is decomposed by its constituents: elastic strain ε^e, plastic strain ε^p and thermal strain ε^{Th}.

Elastic strain is calculated using inverted generalized Hook's law, described by the formulation [19, 21]:

$$\varepsilon_{ij}^e = \frac{1}{E}\left[\left(1+\upsilon\right)\sigma_{ij} - \upsilon\sigma_{kk}\delta_{ij}\right] \tag{8}$$

where E is Young's modulus, v indicates Poisson's ratio and σ_{ij} is the stress tensor and δ_{ij} is the Kronecker delta. Plastic strains are determined on the basis of the model of plastic flow with the Huber-Mises plasticity condition and isotropic strengthening, according to the following equation [19, 21]:

$$f = \sigma_{ef} - \overline{\sigma}\left(\varepsilon_{ij}^p, T\right) = 0 \tag{9}$$

where σ_{ef} is effective stress, $\overline{\sigma}\left(\varepsilon_{ij}^p, T\right)$ is material plasticizing stress – dependent on plastic deformation and temperature.

It is necessary to define the interaction between the two materials for the numerical analysis of laser welding of a lap joint. Heat flow at the contact of joined elements is described by Fourier's law [8, 22]. The boundary condition of the fourth type in the contact of two areas A (sA) and B (sB) has the following form [23]:

$$\lambda_A\left(\frac{\partial T_A}{\partial l_A}\right)_{sA} = \lambda_B\left(\frac{\partial T_B}{\partial l_B}\right)_{sB} \tag{10}$$

$$\textit{when } l < 0 \;\; T_A = T_0 \;\; \textit{or} \;\; l > 0 \;\; T_B = T_0$$

where T_A, T_B are contact temperatures of area A and B [K]; λ_A, λ_B are thermal conductivity coefficients in areas A and B [W/m K]; l is control area between two bodies <–l, l>; sA, sB are surface area.

3. Numerical modelling

The three-dimensional discrete model of the analysed lap joint is developed in Abaqus FEA calculation software. The considered system of the welded joint consists of two dissimilar flat bars made of 304 austenitic steel and S355 steel. The dimensions of analysed system are: $L_1 = L_2 = 50$ mm, $s = 20$ mm, $g_1 = 1$ mm (304 steel), $g_2 = 2$ mm (S355). The flat bars overlap on the length $L_Z = 25$ mm. The diagram of the analysed system is shown in Figure 1.

Figure 2 shows the discrete model of the analysed system developed in Abaqus/CAE software. A much higher density of the finite element mesh is applied in the heat source activity zone due to the large temperature gradients.

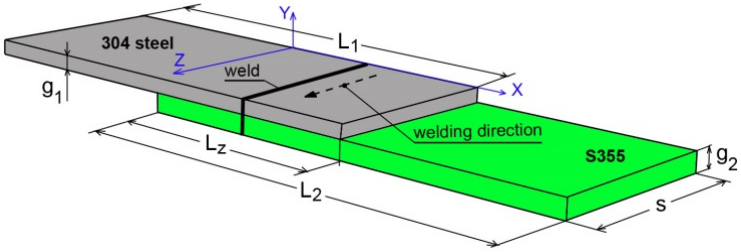

Fig. 1. Scheme of analysed system

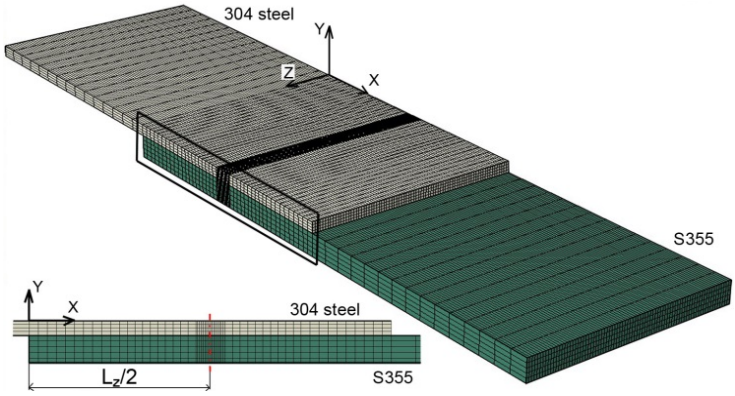

Fig. 2. Scheme of analysed domain with the finite element mesh

Numerical analysis of the overlap welding process in Abaqus software is divided into two stages – the thermal analysis stage and the mechanical analysis stage. The first stage consists in determining the temperature field and determining the shape of the weld pool. The same cuboidal finite elements are used in both thermal phenomena analysis and mechanical phenomena analysis. The difference is the type of elements: DC3D8 elements are used in thermal analysis whereas D3D8R elements are used in mechanical analysis [22]. The heat loss due to radiation, convection and evaporation is assumed, according to Eq. (4). Convection and radiation

heat exchange with the environment is assumed on the remaining surfaces (except for contact planes).

In the case of the analysis of thermal phenomena taking into account contact, it is necessary to define the appropriate interaction conditions (Fig. 3). At the contact of elements in the fusion zone, an ideal contact of two bodies is taken into account, assuming that walls in contact have the same temperatures as well as heat fluxes passing through these walls. On the other hand, in the remaining contact area of joined elements, free contact between surfaces is assumed. A 0.01 mm wide gap is assumed in the area of free contact between the surfaces. The thermal conductivity coefficient is assumed to be linearly variable as a function of the gap width. In order to define this function, two extreme values of the λ coefficient are adopted: for a closed gap (no gap) $\lambda = \lambda^*$, where λ^* is the steel conductivity coefficient and the value of the coefficient at the maximum value of the gap (0.01 mm), $\lambda = \lambda^{**}$, where λ^{**} is the air conductivity coefficient. Figure 3 also contains the boundary mechanical conditions adopted in the numerical calculations. The boundary conditions are selected to ensure the static determinability of the system [17].

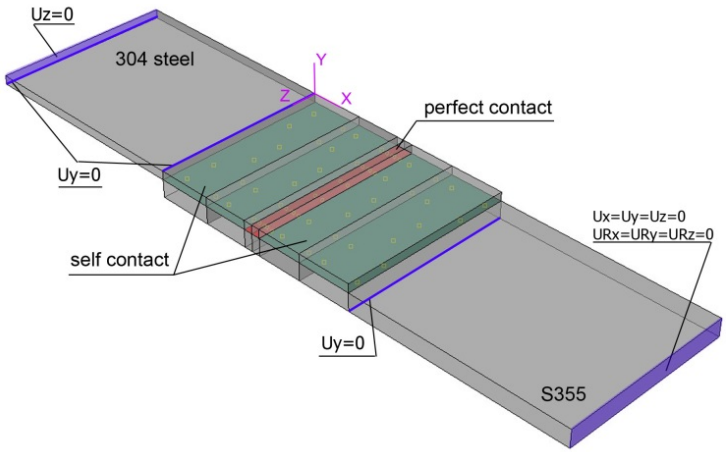

Fig. 3. Scheme of assumed contacts and boundary conditions

In the material module of Abaqus, the mathematical models of two materials have been implemented. Thermomechanical properties of welded materials (Fig. 4) changing with temperature of 304 stainless steel and S355 steels, adapted in simulations, are taken from the literature [15, 17].

Solidus and liquidus temperatures are assumed as follows:

- for S355 steel are set to: $T_S = 1750$ K (1477°C) and $T_L = 1800$ K (1527°C). Latent heat of fusion $H_L = 270 \cdot 10^3$ J/kg;
- for 304 stainless steel are set to: $T_S = 1673$ K (1400°C) and $T_L = 1728$ K (1455°C). Latent heat of equals $H_L = 260 \cdot 10^3$ J/kg.

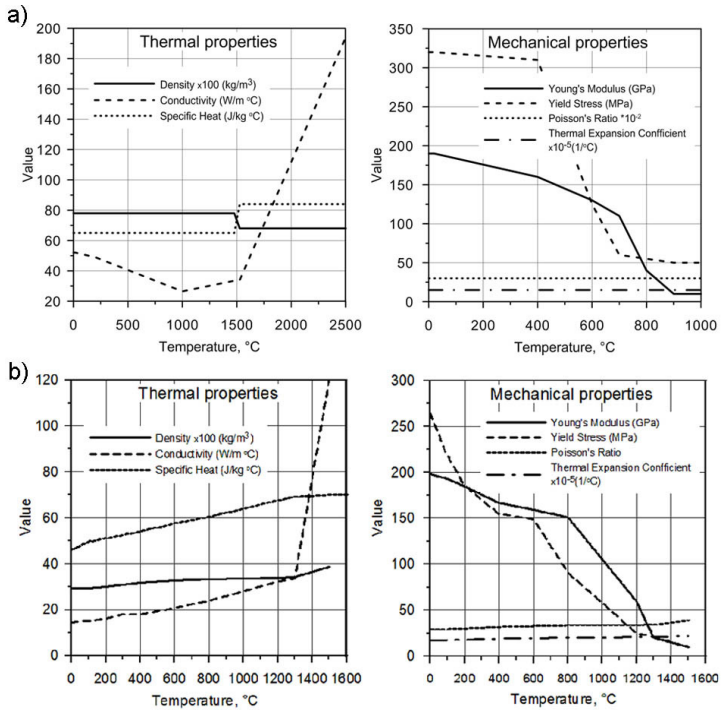

Fig. 4. Thermomechanical properties of welded: a) S355 steel, b) 304 stainless steel

Parameters of the welding process adopted in the calculations are presented in Table 1. The process parameters are estimated on the basis of literature data and numerical verification.

Table 1. Laser welding process parameters

Laser beam power	Efficiency	Welding speed	Beam radius	Penetration deep
3800 W	90%	2 m/min	r_o = 0.3 mm	h = 7 mm

The following parameters are defined for the calculations: the ambient temperature T_o = 293 K (20°C) and convective coefficient α_k = 100 W/m^2 K.

4. Results and discussion

Based on the presented mathematical and numerical model, simulation calculations are carried out in the Abaqus/Standard solving module. Calculations of thermal phenomena are firstly performed on the basis of uncoupled analysis. Figure 5 shows the temperature field in a laser welded lap joint made of dissimilar materials. Figures 5a and 5b show the temperature field for two different simulation times (t = 0.4 s and t = 0.6 s).

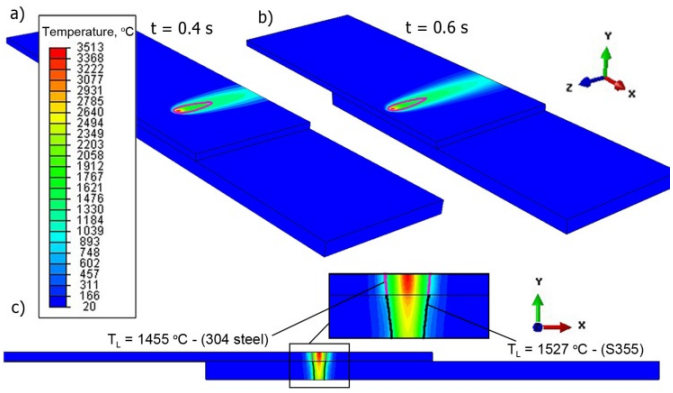

Fig. 5. Temperature distribution (a), general view (b), in the cross section of the laser welded dissimilar materials (c)

The time of laser beam passing through the joint at a speed of 2 m/min is 0.8 s. The total duration of the numerical calculations is 200 s in order to cool down the joint to the correct ambient temperature. In turn, Figure 5c shows the temperature distribution in the cross-section of the joint. The results are presented in the middle of the length of welded materials. A solid line marks the boundaries of the liquid zone for each joined material. The difference between the melting points is about 70°C, which is imperceptible in Figure 5c.

The next figures show the results of the analysis of mechanical phenomena obtained on the basis of the determined temperature field.

Figure 6 shows the numerically estimated reduced stress distributions in the welded lap joint. Figures 6a show the temporary reduced stresses. Figure 6b shows the reduced residual stresses occurring in the joint. The maximum value of these stresses is 251 MPa. Figure 7 shows the reduced residual stresses occurring in a flat bar with a thickness of 2 mm (made of S355 steel). In the comparison of Figures 6b and 7, it can be observed that in a flat bar made of 304 austenitic steel, the stresses are much greater than they are a flat bar made of S355 steel.

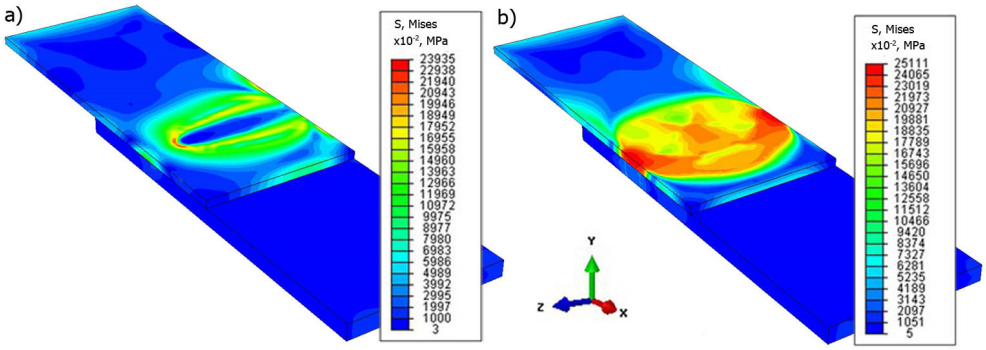

Fig. 6. Residual temporary reduced stress (a) and reduced residual stress (b) of laser welded lap joint

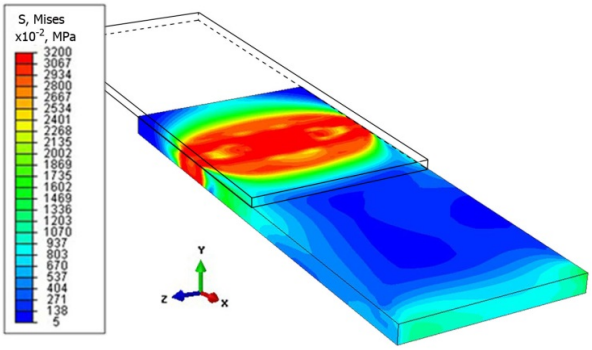

Fig. 7. Reduced residual reduced stress in a flat bar with a thickness of 2 mm

The displacement field is also analysed, as shown in Figure 8. The figure presents displacements averaged along the x-axis direction (U_x) and y-axis direction (U_y). In order to better visualize the deformations resulting from the welding process, U_Y displacement diagrams (Fig. 9) are determined. In the numerically estimated joint, measurement lines are determined separately for a flat bar made of steel 304 and steel S355. Data were taken from the half of the length of the welded lap joint (z = 10 mm) in the direction perpendicular to the weld line.

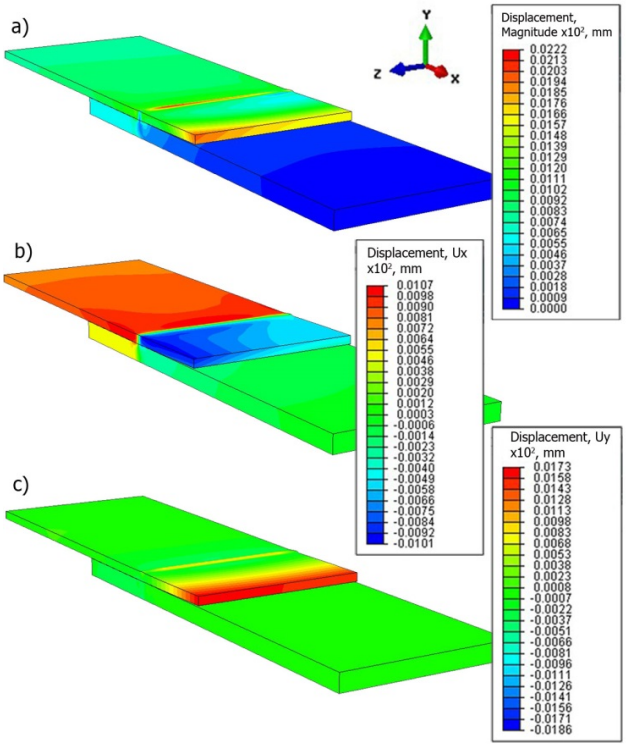

Fig. 8. Displacement fields: a) magnitude, b) U_X, c) U_Y

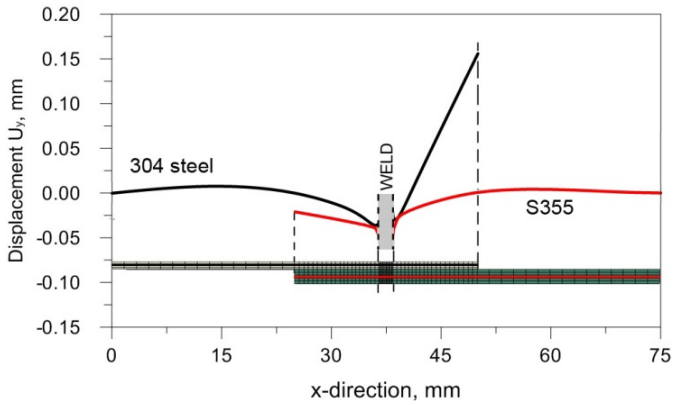

Fig. 9. Numerically estimated deflection U_y

The analysis of U_Y vertical displacement is presented in Figure 8. It can be observed that both flat bars underwent slight deformations. The greatest U_y displacements occur at the upper element (sheet with a thickness of 1 mm) and do not exceed 0.18 mm. Displacements in a 2 mm thick flat bar are much smaller and oscillate around 0.025 mm. The significant difference in the deformation of both flat bars results from the thermal load, acting on the upper element, which is much thinner than the lower one.

5. Conclusions

Joining of two dissimilar materials is a complex process in terms of technology and in development of numerical models. Numerical prediction of thermomechanical phenomena of the welding process using commercial computational software requires development of numerical models taking into account the heating and cooling process of two completely different materials.

The presented article is an effective attempt to build a numerical model describing thermomechanical phenomena occurring in the welding process. The materials adopted in the calculations differ significantly. The only similarity is the melting point of the material (1455°C – 304 austenitic steel and 1527°C – S355 steel). This slight difference can be seen in the temperature distribution in Figure 5c.

The developed numerical model consists of materials of two different thicknesses (1 and 2 mm) and properties. The influence of these differences can be observed in numerically estimated stress and displacement fields. In a flat bar made of 304 stainless steel, 1 mm thick, much higher values of reduced residual stresses can be observed (Figs. 6 and 7), which is also reflected in the displacement field (Figs. 8 and 9). The diagram of displacements in the direction perpendicular to the welding line (Fig. 9) shows that for the adopted dimensions of the analysed model, the maximum value of the displacements U_Y is 0.16 mm and occurs in a flat bar with a thickness of 1 mm. The second joined element also deforms, but to a much

lesser extent. The developed mathematical and numerical models constitute the basis for further research in the field of analysis of overlap welding of joints made of dissimilar materials. The next stage of the research will include the performance of experimental tests and verification of the developed models. On the basis of obtained results of the numerical analysis, it can be concluded that the developed discrete model is universal for different grades of steel presented in the publication. It can be successfully used in the analysis of any welding techniques of materials with various geometries.

References

[1] Moraitis, G.A., & Labeas, G.N. (2008). Residual stress and distortion calculation of laser beam welding for aluminum lap joints. *Journal of Materials Processing Technology*, *198*, 260-269. DOI: 10.1016/j.jmatprotec.2007.07.013.

[2] Pilarczyk J. (2003). Engineer's Guide – Welding Engineering. WNT, Warszawa.

[3] Hietala, M., Järvenpää, A., Keskitalo, M., Jaskari, M., & Mäntyjärvi, K. (2019). Tensile and fatigue properties of laser-welded ultra-high-strength stainless spring steel lap joints. *Procedia Manufacturing*, *36*, 131-137. DOI: 10.1016/j.promfg.2019.08.018.

[4] Wang, H., Wang, Y., Li, X., Wang, W., & Yang, X. (2021). Influence of assembly gap size on the structure and properties of sus301L stainless steel laser welded lap joint. *Materials*, *14*, 996. DOI: 10.3390/ma14040996.

[5] Danielewski, H., & Skrzypczyk, A. (2020). Steel sheets laser lap joint welding – process analysis. *Materials*, *13*(10), 2258. DOI: 10.3390/ma13102258.

[6] Meco, S., Pardal, G., Ganguly, S., Williams, S., & McPherson, N. (2015). Application of laser in seam welding of dissimilar steel to aluminium joints for thick structural components. *Procedia Manufacturing*, *67*, 22-30. DOI: 10.1016/j.optlaseng.2014.10.006.

[7] Chen, L., Wang, Ch., Xiong, L., Zhang, X., & Mi, G. (2020). Microstructural, porosity and mechanical properties of lap joint laser welding for 5182 and 6061 dissimilar aluminum alloys under different place configurations. *Materials and Design*, *191*, 108625. DOI: 10.1016/j.matdes.2020.108625.

[8] Danielewski, H., Skrzypczyk, A., Hebda, M., Tofil, Sz., Witkowski, G., Długosz, P., & Nigrovic, R. (2020). Numerical and metallurgical analysis of laser welded, sealed lap joints of S355J2 and 316L steels under different configurations. *Materials*, *13*(24), 5819. DOI: 10.3390/ma13245819.

[9] Zhong, Y., Xie, J., Chen, Y., Yin, L., He, P., & Lu, W. (2022). Microstructure and mechanical properties of micro laser welding NiTiNb/Ti6Al4V dissimilar alloys lap joints with nickel interlayer. *Materials Letters*, *306*, 130896. DOI: 10.1016/j.matlet.2021.130896.

[10] Yang, B., Zhao, H., Wu, L., Tan, C., Xia, H., Chen, B., & Song, X. (2020). Interfacial microstructure and mechanical properties of laser-welded 6061Al/AISI304 dissimilar lap joints via beam oscillation. *Journal of Materials Research and Technology*, *9*(6), 14630-14644. DOI: 10.1016/j.jmrt.2020.10.064.

[11] Scutelnicu, E., Iordachescu, M., Rusu, C.C., Mihailescu, D., & Ocaña, J.L. (2021). Metallurgical and mechanical characterization of low carbon steel – stainless steel dissimilar joints made by laser autogenous welding. *Metals*, *11*, 810. DOI: 10.3390/met11050810.

[12] Barlas, Z. (2017). Weldability of CuZn30 Brass/DP600 steel couple by friction stir spot welding. *Acta Physica Polonica A*, *132*(3), 991-993. DOI: 10.12693/APhysPolA.132.991.

[13] Shuhai, Ch., Huang, J., Jun, X., Xingke, Z., & Sanbao, L. (2015). Influence of processing parameters on the characteristics of stainless steel/copper laser welding. *Journal of Materials Processing Technology*, *222*, 43-51. DOI: 10.1016/j.jmatprotec.2015.03.003.

[14] http://www.wisconsinwireworks.com/dissimilar_metals.html.

[15] Piekarska, W., Saternus, Z., Kubiak, M., & Domański, T. (2015). Numerical modelling of stress state and deformations in laser butt-welded sheets made of X5CrNi18-10 steel. Metal 2015: 24th International Conference on Metallurgy and Materials, Tanger, 736-741.

[16] Jakubovičová, L., Ftorek, B., Baniari, V., Sapietová, A., Potoček, T., & Vaško, M. (2017). Engineering design of a test device. *Procedia Engineering*, *177*, 520-525. DOI: 10.1016/ j.proeng.2017.02.255.

[17] Kubiak, M., Piekarska, W., Stano, S., & Saternus, Z. (2015). Numerical modelling of thermal and structural phenomena in Yb:Yag laser butt-welded steel elements. *Archives of Metallurgy and Materials*, *60*(2), 821-828. DOI: 10.1515/amm-2015-0213.

[18] Koric, S., & Thomas, B. (2007). *Thermo-mechanical Model of Solidification Processes with ABAQUS.* Abaqus Users Conference, Paris.

[19] Ghafouri, M., Ahn, J., Mourujärvi, J., Björk, T., & Larkiola, J. (2020). Finite element simulation of welding distortions in ultra-high strength steel S960 MC including comprehensive thermal and solid-state phase transformation models. *Engineering Structures*, *219*, 110804. DOI: 10.1016/j.engstruct.2020.110804.

[20] Tsirkas, S.A., Papanikos, P., & Kermanidis Th. (2003). Numerical simulation of the laser welding process in butt-joint specimens. *Journal of Materials Processing Technology*, *134*, 59-69. DOI: org/10.1016/S0924-0136(02)00921-4.

[21] Xu, G., Wu, Ch., Ma, X., & Wang, X. (2013). Numerical analysis of welding residual stress and distortion in laser+GMAW hybrid welding of aluminum alloy T-joint. *Acta Metallurgica Sinica (English Letters)*, *26*(3), 352-360. DOI: 10.1007/s40195-012-0166-5.

[22] Dassault System (2007), Abaqus FEA theory manual. Version 6.7, SIMULIA, USA.

[23] Wiśniewski S., & Wiśniewski T.S. (2012). *Wymiana ciepła*. Warszawa: WNT.